Published in final edited form as:
Neurol Res. 2011 December ; 33(10): 1100–1108. doi:10.1179/1743132811Y.0000000046.

Ammonia-induced brain swelling and neurotoxicity in an organotypic slice model

Adam Back[1], **Kelsey Y. Tupper**[1], **Tao Bai**[1], **Paulpoj Chiranand**[2], **Fernando D. Goldenberg**[1], **Jeffrey I. Frank**[1], and **James R. Brorson**[1]

[1]Department of Neurology, The University of Chicago; 5841 S. Maryland Ave.; Chicago, IL 60637

[2]Section of Ophthalmology, Department of Surgery, The University of Chicago; 5841 S. Maryland Ave.; Chicago, IL 60637

Abstract

Objectives—Acute liver failure produces cerebral dysfunction and edema, mediated in part by elevated ammonia concentrations, often leading to coma and death. The pathophysiology of cerebral edema in acute liver failure is incompletely understood. In vitro models of the cerebral effects of acute liver failure have predominately consisted of dissociated astrocyte cultures or acute brain slices. We describe a stable long-term culture model incorporating both neural and glial elements in a three-dimensional tissue structure offering significant advantages to the study of astrocytic-neuronal interactions in the pathophysiology of cerebral edema and dysfunction in acute liver failure.

Methods—We utilized chronic organotypic slice cultures from mouse forebrain, applying ammonium acetate in iso-osmolar fashion for 72 hours. Imaging of slice thickness to assess for tissue swelling was accomplished in living slices with optical coherence tomography, and confocal microscopy of fluorescence immunochemical and histochemical staining served to assess astrocyte and neuronal numbers, morphology, and volume in the fixed brain slices.

Results—Ammonia exposure at 1–10 mM produced swelling of immunochemically-identified astrocytes, and at 10 mM resulted in macroscopic tissue swelling, with slice thickness increasing by about 30%. Astrocytes were unchanged in number. In contrast, 10 mM ammonia treatment severely disrupted neuronal morphology and reduced neuronal survival at 72 hours by one-half.

Discussion—Elevated ammonia produces astrocytic swelling, tissue swelling, and neuronal toxicity in cerebral tissues. Ammonia-treated organotypic brain slice cultures provide an in vitro model of cerebral effects of conditions relevant to acute liver failure, applicable to pathophysiological investigations.

Keywords

Acute liver failure; ammonia; cerebral edema; organotypic slice culture; optical coherence tomography

Introduction

In acute liver failure (ALF), encephalopathy and life-threatening cerebral edema can occur within hours of a hepatotoxic insult. The sudden cessation of hepatic function has multiple detrimental effects that may contribute to brain dysfunction, including systemic metabolic

Address correspondence to: Dr. James R. Brorson, Department of Neurology, MC2030, The University of Chicago, 5841 S. Maryland Ave. Chicago, IL 60637, Ph: 773-702-7215, Fax: 773-702-9076, jbrorson@neurology.bsd.uchicago.edu.

dysfunction, accumulation of circulating toxins, and decreased protein synthesis with accompanying brain hemorrhage risk. Among the derangements associated with ALF, accumulation of ammonia has often been implicated as the primary mediator in the cerebral dysfunction and edema that can be the cause of death in these patients [1, 2]. Normal human arterial concentrations of total ammonia (primarily in the form of the ammonium ion at physiological pH) are found in the range of 30–80 μg/dL, while in human ALF, arterial ammonia levels can range from 200–2000 μg/dL. Such levels correspond to low millimolar concentrations (1 mM ~ 1700 μg/dL). Evidence that ammonia is a primary mediator of toxic effects of ALF on the brain comes from clinical observations, whole animal models, and cell culture studies. Serum ammonia accumulation is a direct and rapid result of hepatic urea cycle dysfunction, and in animal models of ALF, brain ammonia can rise to 5 mM [3]. In addition, rare patients with primary urea cycle disorders can develop extreme hyperammonemia in the absence of global liver dysfunction, and the accompanying brain swelling and dysfunction can be rapidly ameliorated by measures to reduce serum ammonia [4]. Direct application of elevated ammonia to dissociated cultures of astrocytes has been shown to produce astrocytic swelling [3, 5], and infusion of ammonium acetate in rats produces brain edema, astrocytic enlargement, and ultrastructural alterations [6, 7].

The question of how ALF in general, and hyperammonemia in particular, can lead to cerebral edema is not fully answered. In animal models of ALF, cytotoxic edema in astrocytes has been observed. In astrocytes, glutamate and ammonia are converted by glutamine synthetase to glutamine [7]. Intracellular glutamine has been postulated to constitute an osmotic intracellular load, driving intracellular water accumulation and cytotoxic edema [3]. More recent evidence has drawn attention to intracellular glutaminase-mediated metabolism of glutamine, producing glutamate and ammonia, and resulting in ammonia-induced disruption of mitochondrial function, with activation of the mitochondrial permeability transition and metabolic failure [8]. Other mechanisms have also been proposed as possible mediators of cerebral swelling and dysfunction in ALF. These include excitotoxicity due to extracellular accumulation of the excitatory neurotransmitter glutamate, accumulation of active CNS depressants such as endogenous benzodiazepines, generation of circulating inflammatory mediators such as TNFα, alterations in cerebral blood flow, and dysfunction of the membrane water channel aquaporin-4 [1, 9, 10, 11]. It is likely that clinical brain dysfunction in ALF is multifactorial, with multiple toxins working in concert. Nevertheless, evidence for the key role of ammonia is widely accepted.

Animal models of cerebral effects of acute liver failure have utilized dogs, rabbits, rats, or mice, with induced liver failure through hepatic devascularization, hepatectomy, or treatment with hepatotoxins including acetaminophen, thioacetamide, and galactosamine [12]. Some models are hampered by variability in observations of hepatic encephalopathy or brain edema, and by features not routinely seen in human ALF such as brain necrosis. All animal models are limited by the expense and difficulty involved in whole animal treatments, and the lack of ready access to brain tissues for continuous observation or treatment during hepatic encephalopathy. Nevertheless, whole-animal models have been a mainstay in the elucidation of pathology and pathophysiology of cerebral effects of ALF.

In vitro models have to date consisted primarily of dissociated rat cortical astrocyte cultures or acute brain slices [12]. These models have contributed important insights into the pathophysiology of ALF, including, for example, confirmation that excess ammonia concentrations produce astrocyte swelling and mitochondrial dysfunction [5]. However, recognized deficiencies in these models exist, in that dissociated astrocyte cultures lack other cellular elements of brain tissue and eliminate the three-dimensional spatial relationships of astrocytes and neurons that may be key to their interactions and dysfunction. Furthermore, dissociated astrocytes continuously proliferate and thus are not stable for long-

term experiments. Similarly, acute brain slices are viable in vitro only for several hours, whereas brain pathology is observed to develop over 1–3 days. A recent consensus statement from a commission of the International Society for Hepatic Encephalopathy and Nitrogen Metabolism called for models incorporating the preserved tissue architecture and multiple cell types of the cerebrum [12].

Here we report the use of ammonia-treated organotypic brain slice cultures as a model of cerebral edema in ALF. Organotypic slice culture offers several advantages over dissociated cell culture, including the presence of both neurons and astrocytes, the preservation of the three-dimensional tissue structure of the brain, the ability to distinguish cortical from subcortical and white matter brain areas, and stability of the cultured tissue for weeks [13]. The neuronal/astrocytic contacts that are of known importance to metabolism and to tissue fluid and electrolyte homeostasis are preserved. The in vitro exposure of the cultured brain slice allows ready application of pharmacological and molecular treatments, for mechanistic investigations of brain effects of simulated ALF.

Using this approach, we report that organotypic brain slices treated with ammonia for 3 days show evidence of tissue edema that is linked with astrocytic swelling. Astrocytes are preserved in number. Neurons, however, are diminished in number and display disrupted morphology after ammonia exposure, with both swollen cell profiles and shrunken cells with pyknotic nuclei in evidence. These results confirm that ammonia at high concentrations produces cytotoxic edema in astrocytes, and also demonstrate direct neuronal injury from elevated ammonia.

Methods

Organotypic brain slice cultures and treatments

Post-natal day 2 pups of C57BL/6 mice, purchased from Charles River Laboratories, were anesthetized with isoflurane, cervically decapitated, and dissected. Whole brain tissue samples were transferred in Gey's Balanced Salt Solution at −20°C to a McIlwain tissue chopper (Mickle Laboratory Engineering Co, Surrey, England), and sectioned at 385 μm intervals in the coronal plane, obtaining from each brain four sections, from 770 μm to 2310 μm caudal to the frontal pole, including frontal cortex and rostral diencephalon. Brain sections were placed on 0.4 μm Millicell-CM culture plate inserts (Millipore) within wells of a six-well plate, with 2 or 3 sections per well, in 1 ml of culture media (MEM plus 25% horse serum, 25% Hanks' Balanced Salt Solution, supplemented with 6.4 mg/ml of glucose and 2 mM of L-glutamine). Slices rested at the gas-fluid interface. Cultures were incubated at 37°C with 5% CO_2 and fed biweekly by exchanging half the culture media per well.

After two weeks in culture, slices were treated with ammonium acetate at concentrations of 1–30 mM, with 10 or 30 mM sodium acetate serving as a control. This was administered in an iso-osmolar fashion, by diluting a 150 mM stock solution of ammonium acetate or of sodium acetate to twice the highest target concentration in culture medium, followed by readjustment of pH to 7.4 as required, and then by replacement of half of culture medium in culture wells with the iso-osmolar ammonium acetate or sodium acetate solution. Treatments were applied for 72 hours.

Slice imaging and Optical Coherence Tomography

Serial images of cultured slices were acquired using a ChemiGenius Bio Imaging System (Syngene, Frederick, MD, USA). Images were calibrated and slice areas measured using NIH ImageJ software. For measurement of thickness of cultured slices, optical coherence tomography (OCT) was applied utilizing the Zeiss Stratus OCT machine. Cultured slices were washed and transported in a physiological ice-cold saline (145 mM NaCl, 3 mM KCl,

2 mM $CaCl_2$, 1 mM $MgCl_2$, 10 mM HEPES, pH 7.4). Culture well inserts were removed from culture plates and placed in a chilled saline-filled clear imaging chamber mounted vertically in the viewing area of the OCT machine. A line-scan imaging mode was used in which a cross-sectional image of the slice thickness was obtained in a 7.5 mm horizontal line across the upper cortex of the slice, at a position approximately two-thirds up from the ventral surface towards the dorsal cortical surface. Polarization was optimized to obtain the clearest OCT image, and a single optimized cross–sectional image was collected for each slice in the culture well.

Image analysis was performed in a blinded fashion. Image files were imported into NIH ImageJ software application. The fixed image width was used for calibration, and the thickest cross-sectional dimension was measured in the cortex of each hemisphere, using the line drawing tool in ImageJ, in a transect perpendicular to the supporting membrane. As the boundary between the supporting membrane and the tissue slice was indistinct, the membrane was included in the measurement, with subsequent subtraction of the uniform membrane thickness of 50 microns. Thickness values from the two hemispheres within each slice, and from all slices from the same well, were averaged together to give a single value for each treatment condition in each independent replicate.

Immunostaining and histochemical staining

Tissue slices were fixed in 4% paraformaldehyde for 20 minutes at 37°C, followed by washing in phosphate buffered saline (PBS), three times for 10 minutes each, with all washes on a rotating platform. Next the tissue was permeabilized in 0.1% Triton/PBS for 10 minutes, washed twice more, and then placed in blocking buffer (1.5% normal donkey serum in 0.1% Triton/PBS) for 24 hours at 4°C. Following blocking, the slices were excised from culture well inserts on a fragment of the supporting membrane for subsequent staining.

For immunostaining, monoclonal anti-glial fibrillary acidic protein (GFAP) antibody (1:300 dilution; Neomarkers; Fremont, CA) was applied in blocking buffer for 24–48 hours at 4°C. Tissue slices were washed three times in PBS for 10 minutes, followed by application of Cy5-anti mouse IgG as secondary antibody (1:250; Jackson ImmunoResearch, West Grove, PA) for 24 hours at 4°C. Following washing in PBS, tissues were then counterstained with Hoechst 33342 dye diluted 1:1000 in PBS for 20 minutes, washed twice in PBS, and then mounted. Specific staining of neurons used the fluorescent Nissl stain Fluoro-Nissl Green (Molecular Probes-Invitrogen). After fixation and washing in PBS, slices were incubated in Fluoro-Nissl Green (1:300) and Hoechst dye 33342 (1:2000) in PBS, for 20 minutes, followed by washing in PBS twice for 10 minutes, and then for 24 hours. Stained tissue slices, attached to supporting membrane fragments, were whole mounted on glass slides under thin glass coverslips in Fluoromount-G (Southern Biotech, Birmingham, AL).

Immunoblotting

Tissue slices were rinsed with ice-cold PBS and harvested in tissue lysis buffer (50 mM Tris-HCl, pH 7.4, 150 mM NaCl, 5 mM EDTA, 0.1% SDS, 2 mM Na_3VO_4) containing protease inhibitor cocktail (Roche Applied Science, Indianapolis, IN, USA). The lysates were sonicated and then centrifuged at 16,000 *g* at 4°C for 20 min. Protein concentrations of the supernatants were measured with bicinchoninic acid (BCA) protein assay (Thermo Scientific Pierce, Rockford, IL, USA). Twenty to thirty μg of total protein was loaded onto 10% SDS-PAGE gels and transferred onto nitrocellulose membranes (Protran, Whatman GmbH, Germany). Blots were probed with anti-GFAP monoclonal antibody (anti-GFAP mAb, 1:5000, Sigma-Aldrich, St. Louis, MO) followed by horseradish peroxidase-conjugated goat anti–mouse IgG (Bio-Rad Laboratories, Hercules, CA). Anti-β-actin (Sigma) was used as a loading control. Blots were developed with an enhanced

chemiluminescence detection kit (Thermo Scientific Pierce) and imaged by the Bio Imaging System. Bands were quantified using Genesnap software (Syngene).

Microscopy and Image Data Analysis

A DSU spinning disc confocal microscope (Olympus DSU Spinning Disk Confocal Microscope) was used to acquire 3D stack images for each treatment. Two image stacks were acquired per slice (one per cerebral hemisphere). At low power (2x objective), a standard area of dorsal cortex was located and centered in the microscopic field (see Figure 2A). Next, under a 60X water-immersion objective, the dorsal pial margin of the cortex was located, and an imaging field was selected approximately 150 microns in along a perpendicular line from the pial surface. The focal plane of the upper surface of the slice was located, and the initial optical section in the z-axis was set to begin at approximately 2 microns depth from the surface. Image stacks of 12 optical sections, each of 1 micron in thickness, were acquired in appropriate wavelength channels. The number of astrocytes was counted in GFAP immunostaining image stacks. Automatic thresholding was then applied to image stacks in the NIH ImageJ program, with fixed settings across images, to produce a 3-dimensional template corresponding to positive GFAP immunoreactivity. Using a voxel counter plug-in, the number of immunopositive voxels, as well as the mean immunostaining intensity, were then computed for each image stack.

Neuronal counts from image stacks were also obtained from Fluoro-Nissl-stained slices. The standard area of dorsal cortex was again located as described above. A larger volume of cortex was imaged for neuronal counting, with a confocal z stack starting at the slice surface and extending to a depth of 30 microns, with fifteen images acquired at 2 microns intervals, yielding a three-dimensional image stack of 138 x 138 x 30 micron. Using the ImageJ Cell Counter plug-in to mark counted objects, Fluoro-Nissl-positive cell bodies, centered around Hoechst-stained nuclei, were counted in a blinded fashion in the three dimensional image stacks, following stereological principles to eliminate duplicative counting of objects. The counts from bilateral hemispheric sampling areas were averaged for each treatment condition in each replicate, and normalized to the mean counts across condition within each replicate.

Statistics

Experiments were performed in 4–8 independent replicates. Results are presented graphically as mean ± S.D. One-way ANOVA testing, with $p<0.05$, was used to discern significance, followed by post-hoc pairwise testing.

Results

Treatment of Organotypic brain slice cultures with ammonium acetate

Organotypic slice cultures from forebrain areas of newborn mice were generated and stabilized in culture for 2–3 weeks. Cultured slices maintained recognizable gross anatomical features, with identifiable separation between cortex and subcortical structures. Previous studies have shown preservation of identifiable laminar distribution of pyramidal neurons within the cortical gray matter of such organotypic cultured slices [14].

At 2 weeks, brain slices were exposed to ammonium acetate in a range of concentrations from 0–10 mM, as well as to Na acetate as control for 3 days, with treatments applied in iso-osmolar fashion. With exposure to the higher ammonia concentrations, slices became visibly less translucent (Figure 1A), with an appearance grossly suggesting tissue swelling. To assess for any lateral tissue swelling in the plane of the membrane, serial photographs of

cultured slices were analyzed for changes in slice area. No significant changes in slice area were detected over 3 days at ammonia concentrations up to 10 mM (Figure 1B).

Accurate determination of slice thickness was undertaken using optical coherence tomography (OCT), a technology most commonly employed for retinal imaging in clinical settings. Treated slices were removed from the culture environment, washed, and placed in ice-cold physiological saline. OCT cross-sectional images of individual slices were obtained in a horizontal line scan across the dorsal portion of slices (Figure 1C). Control slices were generally somewhat reduced in thickness from the initial value of 385 microns. All slices were markedly thicker in cortical gray matter areas than in subcortical white matter areas. Blinded analysis of maximal cortical thickness in treated slices revealed that treatment with 10 mM ammonia produced a significant increase in average maximal slice thickness to 441 ± 40 microns, approximately 30% greater than thickness of control slices (345 ± 33 microns) (Figure 1D). In contrast, iso-osmolar 10 mM Na acetate treatment produced no measureable change, ruling out the possibility that swelling induced by ammonium acetate was a non-specific effect of acetate exposure. Thus iso-osmolar ammonia exposure, at 10 mM, produced substantial tissue swelling over 3 days in cultured brain slices.

GFAP-immunostained astrocytes in ammonia-treated brain slice cultures

Studies in dissociated cell culture have suggested that ammonia-induced swelling may occur primarily in astrocytes [15]. To explore the cellular basis for brain tissue swelling in cultured slices, treated slices were fixed and immunostained for glial fibrillary acidic protein (GFAP), a cytoskeletal protein specific for astrocytes. Whole-mounted immunostained slices were imaged by confocal methods in a standardized fashion, sampling a pre-determined volume (138 x 138 x 12 microns) of dorsal cortex (Figure 2A) for GFAP immunoreactivity, with 1.0 micron optical sectioning. Astrocytes appeared as brightly stained profiles with stellate shape (Figure 2B, C). The intensity of GFAP immunostaining appeared to be greater after treatment with ammonia 1–10 mM than in control slices. GFAP- immunoreactive astrocytes were counted throughout the sampled volume, with no significant change in the number of astrocytes over ammonium concentrations of 1 – 10 mM (Figure 2D). To evaluate for astrocytic swelling, the volume of GFAP-immunoreactivity was used as a marker of astrocyte cytoplasmic volume. A standardized image analysis protocol was applied to the stacks of confocal images of GFAP-immunostained slices, with thresholding of images for fluorescence above background, followed by evaluation for total volume of immunoreactive voxels. The fractional volume of cortex occupied by GFAP-immunoreactive voxels progressively and significantly increased at concentrations of 1–10 mM ammonia, but was not increased by 30 mM Na acetate, in comparison to control samples (Figure 2E). Of note, the measured net increase in GFAP-immunoreactive volume at 10 mM ammonia was approximately 8% of the total tissue volume, accounting for a substantial fraction of the overall tissue swelling indicated by direct measurement of tissue volume by OCT.

Slices were also harvested for tissue lysis after ammonia treatment, and subjected to Western blotting for GFAP (Figure 3). No statistically significant change in GFAP content, normalized to β-actin, was evident after exposure of slices to 1–10 mM ammonia, with a trend toward decreased GFAP content at 10 mM, suggesting that the increase in volume of GFAP immunoreactivity with increasing ammonia concentrations is more likely due to swelling than to astrocytic growth, and that the qualitatively brighter immunohistochemical staining for GFAP observed at higher ammonia concentrations must be attributed to an unmasking of epitopes with cell swelling, rather than to an increase in GFAP expression. At 30 mM ammonia, intact protein bands for both GFAP and β-actin were diminished, consistent with tissue breakdown.

Neuronal changes in ammonium-treated brain slices

To identify neurons within the treated brain slices, the neuron-specific stain Fluoro-Nissl was applied, along with staining of nuclei by the DNA stain Hoechst 33342, followed by confocal imaging. Again, a standardized imaging protocol was applied to a consistent volume of dorsolateral cortex in the slices. Qualitatively, neurons in control slices were stained brightly with the Fluoro-Nissl dye in a somatic cytoplasmic pattern, with no detectable staining of neurites or nuclei (Figure 4A). Neurons were numerous, greatly outnumbering the Nissl stain-negative cells present in the slices, and outnumbering the prior astrocyte counts (see 2D, above). In control and Na acetate-treated slices, neurons were relatively uniform in somatic size, 10–15 microns in somatic diameter, and contained large round or oval nuclei with non-condensed chromatin. In contrast, in slices treated with 10 mM ammonia for 3 days, the Fluoro-Nissl-stained neurons were variable in size, with some enlarged to 20 microns or more in somatic diameter, associated with large swollen nuclei, while others were shrunken and irregular in shape, with pyknotic nuclei (Figure 4B). Many pyknotic nuclei lacked associated Fluoro-Nissl-staining cytoplasm. Qualitatively, identifiable neurons (with residual Nissl staining) were variably reduced in number, and this was confirmed quantitatively by blinded counting of neurons within three-dimensional imaged volumes (Figure 4C), with neuron numbers decreased by about one-half after treatment with 10 mM ammonia, as compared to control slices.

Discussion

Acute liver failure leads to devastating cerebral effects, including potentially lethal cerebral edema. Mechanistic studies of these cerebral effects have primarily relied upon dissociated astrocyte cultures or upon more complex whole animal studies with induced liver failure. Here we describe initial features of a model of cerebral effects of elevated ammonia, simulating acute liver failure, on brain tissue in chronic organotypic brain slices. This model preserves the tissue architecture and close cell-cell contacts between astrocytes and neurons that may be crucial to metabolism, cell volume regulation, and cell survival in brain tissue. It offers the ability to observe both astrocytes and neurons directly, through confocal microscopy, in brain tissue, with the usual advantages of the in vitro setting in terms of control over the chemical milieu and ease of manipulation.

Using this model, we have found that elevated ammonia, applied in iso-osmolar fashion, is sufficient to produce substantial gross tissue swelling and microscopic astrocytic swelling, and to lead to neuronal degradation. Elevated ammonia alone, without other factors associated with liver failure, has previously been shown to be sufficient in astrocyte cultures to produce astrocytic swelling and metabolic disruption [16, 17], but in vitro models have generally not included the brain tissue structure that organotypic slice cultures provide, allowing an assessment of the overall tissue swelling. In ALF, the progressive brain swelling poses an immediate threat to survival. In the present model, gross tissue swelling amounted to nearly 30% at 10 mM ammonia. To put this in a clinical perspective, this exceeds the total proportion of the rigidly enclosed intracranial volume occupied by the CSF and blood compartments capable of undergoing some degree of compensatory decrease in volume to accommodate brain tissue swelling, so that fatal elevation of intracranial pressure would precede this degree of swelling. In vivo models of ammonia- induced brain edema, measured as changes in tissue specific gravity, have reported somewhat lesser maximal increases in total tissue water content, in the range of 7 – 12% [6]. Presumably important differences attributable to the in vivo setting, possibly including the limiting effect of intracranial pressure elevations on tissue water accumulation, may account for lesser swelling in vivo than is found in the present in vitro model.

While this model of ammonia-induced cerebral swelling offers distinct advantages over previous in vitro models, some clear limitations must also be recognized. It shares with other in vitro models the lack of vascular delivery system and of the blood brain barrier. The blood-brain barrier interposes the astrocytic endfeet between the blood and brain extracellular compartment, and might be expected to modulate the direct delivery of ammonia to the brain through astrocytic metabolism of ammonia to glutamine [15]. However, a recent study in hepatectomized pigs with elevated arterial ammonia confirmed that microdialysis-measured extracellular brain ammonia concentrations, while lagging behind those in the blood, reached low millimolar levels within 16 hours of liver failure [18]. This would suggest that exposure of brain slices to elevated ammonia bears direct relevance to the pathophysiological state in ALF in vivo. However, vasogenic factors play an increasingly recognized role in producing brain edema in ALF, with vasogenic edema from disruption of blood-brain barrier and extravasation of blood-borne solutes preceding cytotoxic edema in rodent in vivo models [19, 20]. The lack of incorporation of vascular elements in the present model thus presents a notable limitation.

It should be further noted that in the present model macroscopic tissue swelling could only be confirmed at 10 mM ammonia, a concentration substantially higher than that commonly encountered in clinical liver failure. Immunostaining of astrocytes indicated significant microscopic swelling at 1–3 mM, suggesting that the threshold for ammonia-induced changes in this model might be at lower, more clinically relevant concentrations. Nevertheless, the important possibility also is raised that ammonia alone, at clinically relevant concentrations, is not sufficient to produce brain tissue swelling. Other factors commonly present in acute liver failure, such as release of inflammatory mediators, may combine with ammonia accumulation to trigger potentially fatal brain swelling. The present model facilitates testing of this hypothesis, allowing controlled co-application with ammonia of cytokines such as TNF-α, implicated in the pathophysiology of hepatic encephalopathy [21].

In addition to the astrocytic swelling observed in this model, a severe neurotoxic effect of 10 mM ammonia was evident. Studies in neurons in dissociated cultures have previously documented the direct neurotoxicity of ammonia, involving apoptotic, excitotoxic, and oxidant mechanisms [22, 23, 24]. However, the presence of co-cultured astrocytes in moderate numbers was found to be sufficient to protect cultured neurons from damage by 5 mM ammonia [24], suggesting that similar protection of neurons by surrounding astrocytes might occur in vivo. Classical neuropathological descriptions of brain changes in hepatic encephalopathy have emphasized the changes in glia over those in neurons, and generally clinical observations have suggested that irreversible neural damage does not result from brief exposure to hyperammonemia alone unless brain edema and intracranial pressure elevation produce secondary injury [8]. However, it has been proposed that some of the movement abnormalities and cognitive sequelae of liver failure that persist after liver transplantation or recovery may reflect direct neuronal injury, with limited experimental data addressing the issue of neuronal cell death in models of acute liver failure [25]. The toxicity to neurons demonstrated in the present model at the highest ammonia concentrations occurred despite the presence of astrocytes in close anatomical contact. This result may be an artifact of the model, utilizing ammonia concentrations exceeding those occurring in hyperammonemic states. Nevertheless, it raises concerns that some neurotoxicity may result not only from effects of tissue swelling and elevated intracranial pressure, but also from direct injury by ammonia to neurons, at least when very high ammonia levels are sustained for days.

Organotypic brain slices offer the opportunity to study the mechanisms underlying ammonia-induced astrocytic swelling and neurotoxicity in intact neural tissues containing

both neuronal and astrocytic elements, and with the potential to use pharmacological, molecular, and genetic tools in experimental protocols. Confocal imaging techniques like those demonstrated here can also be extended to the study of living tissues, with fluorescence indicators or fluorescently labeled organelles allowing physiological studies of effects of ammonia on intracellular ionic concentrations or on mitochondrial morphology and membrane potential. Such studies may provide new insights into treatment approaches for cerebral edema and dysfunction in acute liver failure.

Acknowledgments

We wish to thank Vytautas Bindokas at the University of Chicago Imaging Core facility for his support with image acquisition and processing, and Simren Dulai for assistance with slice cultures and staining. We also wish to acknowledge with gratitude the guidance provided of the late Andres Blei in the conception of this project, and the generous support of the Greenwood Trust. This work was supported by a Preclinical Pilot Translational Award to J.B., granted under a Clinical Translational Science Award to the University of Chicago (3UL1 RR024999-03S; Solway, P.I.).

References

1. Norenberg MD. Astroglial dysfunction in hepatic encephalopathy. Metab Brain Dis. 1998; 13:319–335. [PubMed: 10206824]
2. Kundra A, Jain A, Banga A, et al. Evaluation of plasma ammonia levels in patients with acute liver failure and chronic liver disease and its correlation with the severity of hepatic encephalopathy and clinical features of raised intracranial tension. Clin Biochem. 2005; 38:696–699. [PubMed: 15963970]
3. Swain M, Butterworth RF, Blei AT. Ammonia and related amino acids in the pathogenesis of brain edema in acute ischemic liver failure in rats. Hepatology. 1992; 15:449–453. [PubMed: 1544626]
4. Wendell LC, Khan A, Raser J, et al. Successful management of refractory intracranial hypertension from acute hyperammonemic encephalopathy in a woman with ornithine transcarbamylase deficiency. Neurocrit Care. 2010; 13:113–117. [PubMed: 20422467]
5. Rama Rao KV, Norenberg MD. Aquaporin-4 in hepatic encephalopathy. Metab Brain Dis. 2007; 22:265–275. [PubMed: 17879149]
6. Hilgier W, Olson JE. Brain ion and amino acid contents during edema development in hepatic encephalopathy. J Neurochem. 1994; 62:197–204. [PubMed: 8263520]
7. Willard-Mack CL, Koehler RC, Hirata T, et al. Inhibition of glutamine synthetase reduces ammonia-induced astrocyte swelling in rat. Neurosci. 1996; 71:589–599.
8. Norenberg MD, Rama Rao KV, Jayakumar AR. Ammonia neurotoxicity and the mitochonfdrial permeability transition. J Bioenerg Biomembr. 2004; 36:303–307. [PubMed: 15377862]
9. Bai G, Rama Rao KV, Murthy CRK, et al. Ammonia induces the mitochondrial permeability transition in primary cultures of rat astrocytes. J Neurosci Res. 2001; 66:981–991. [PubMed: 11746427]
10. Blei AT. The pathophysiology of brain edema in acute liver failure. Neurochem Int. 2005; 47:71–77. [PubMed: 15961187]
11. Jalan R. Pathophysiological basis of therapy of raised intracranial pressure in acute liver failure. Neurochem Int. 2005; 47:78–83. [PubMed: 15927306]
12. Butterworth RF, Norenberg MD, Felipo V, et al. Experimental models of hepatic encephalopathy: ISHEN guidelines. Liver Int. 2009; 29:783–788. [PubMed: 19638106]
13. Gähwiler BH, Capogna M, Debanne D, et al. Organotypic slice cultures: a technique has come of age. Trends Neurosci. 1997; 20:471–477. [PubMed: 9347615]
14. Young KC, McGehee DS, Brorson JR. Glutamate receptor expression and chronic glutamate toxicity in rat motor cortex. Neurobiol Dis. 2007; 26:78–85. [PubMed: 17240155]
15. Rama Rao KV, Jayakumar AR, Norenberg MD. Differential response of glutamine in cultured neurons and astrocytes. J Neurosci Res. 2005; 79:193–199. [PubMed: 15573403]

16. Norenberg MD, Baker L, Norenberg L-OB, et al. Ammonia-induced astrocyte swelling in primary culture. Neurochem Res. 1991; 16:833–836. [PubMed: 1944774]

17. Rama Rao KV, Jayakumar AR, Norenberg MD. Induction of the mitochondrial permeability transition in cultured astrocytes by glutamine. Neurochem Int. 2003; 43:517–523. [PubMed: 12742099]

18. Zwirner K, Thiel C, Thiel K, et al. Extracellular brain ammonia levels in association with arterial ammonia, intracranial pressure and the use of albumin dialysis devices in pigs with acute liver failure. Metab Brain Dis. 2010; 25:407–412. [PubMed: 21086032]

19. Nguyen JH, Yamamoto S, Steers J, et al. Matrix metalloproteinase-9 contributes to brain extravasation and edema in fulminant hepatic failure mice. J Hepatol. 2006; 44:1105–1114. [PubMed: 16458990]

20. Cauli O, López-Larrubia P, Rodrigo R, et al. Brain region-selective mechanisms contribute to the progression of cerebral alterations in acute liver failure in rats. Gastroenterology. 2011; 140:638–645. [PubMed: 20977905]

21. Odeh M. Pathogenesis of hepatic encephalopathy: the tumour necrosis factor-α theory. Eur J Clin Invest. 2007; 37:291–304. [PubMed: 17373965]

22. Yang L, Omori K, Omori K, et al. $GABA_C$ receptor agonist suppressed ammonia-induced apoptosis in cultured rat hippocampal neurons by restoring phosphorylated BAD level. Journal of Neurochemistry. 2003; 87:791–800. [PubMed: 14535961]

23. Klejman A, Wegrzynowicz M, Szatmari EM, et al. Mechanisms of ammonia-induced cell death in rat cortical neurons: Roles of NMDA receptors and glutathione. Neurochem Int. 2005; 47:51–57. [PubMed: 15985217]

24. Rama Rao KV, Panickar KS, Jayakumar AR, et al. Astrocytes protect neurons from ammonia toxicity. Neurochem Res. 2005; 30:1311–1318. [PubMed: 16341593]

25. Butterworth RF. Neuronal cell death in hepatic encephalopathy. Metab Brain Dis. 2007; 22:309–320. [PubMed: 17851742]

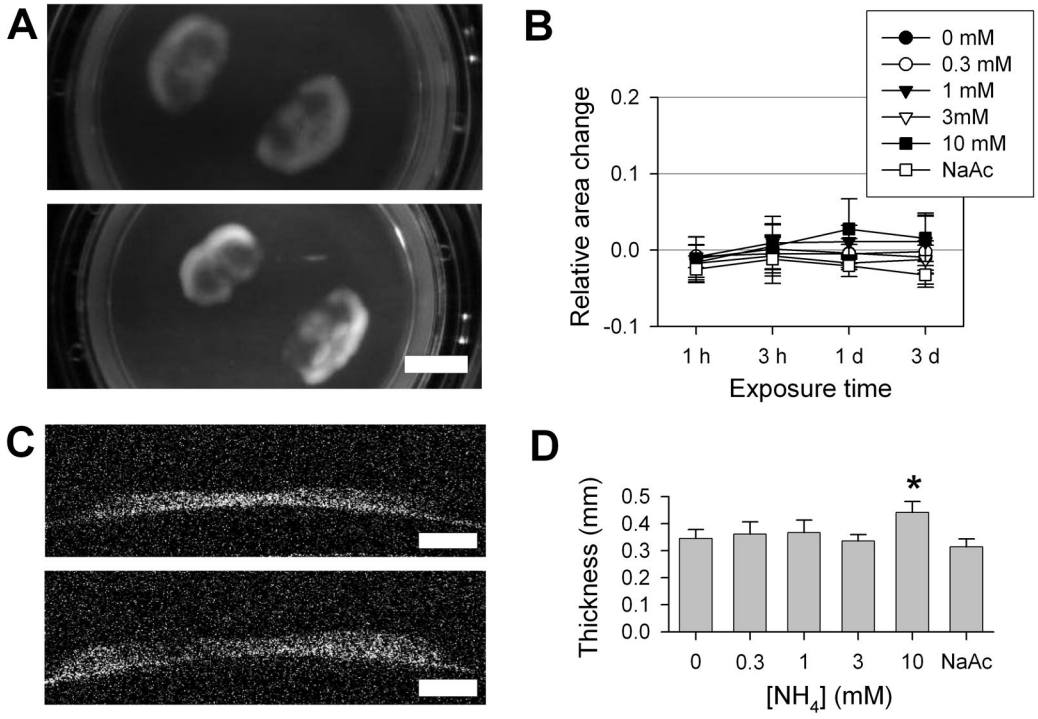

Figure 1. Ammonia-induced tissue swelling in cultured brain slices

A) Representative photographs of cortical organotypic cultured slices, after 3 day treatments in control conditions or with 10 mM NH_4 acetate (scale, 5 mm). B) Relative change in measured areas of slices treated with NH_4 acetate, 0–10 mM, or 10 mM Na acetate (NaAc), over 3 days (n = 5; mean ± S.D.). There were no significant differences found between treatment conditions. C) Optical coherence tomography cross-sectional images of cultured brain slices, adherent to the supporting membrane, after 3 day treatments with control or 10 mM NH_4 conditions (scale, 1 mm). D) Slice thickness after 3 days treatment with NH_4 acetate, 1–10 mM, or with 10 mM Na acetate (n = 4, mean ± S.D.). At 10 mM NH_4, average slice thickness was significantly increased (*$p < 0.01$).

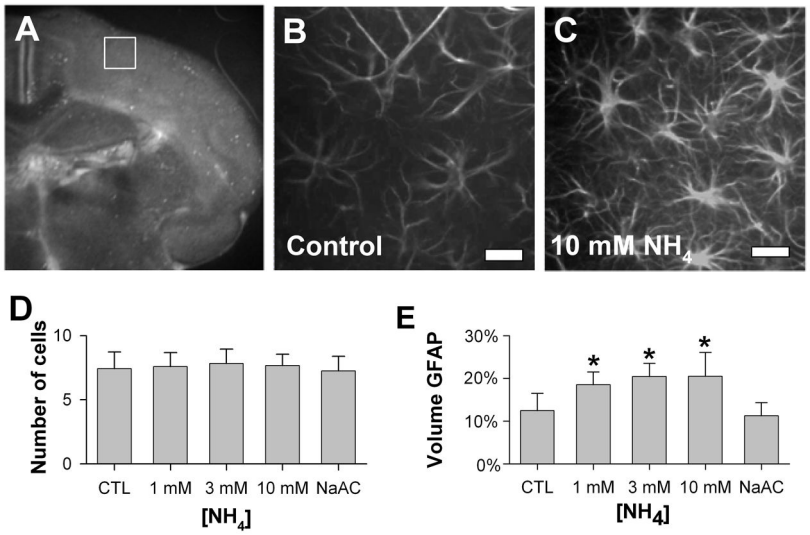

Figure 2. Astrocytes in ammonia-treated cultured brain slices

A) Low-power fluoro-micrograph of Hoechst-stained cultured organotypic slice, showing the standard imaging sampling area in dorsolateral cortex (white box). B), C) Representative confocal optical sections of GFAP-immunoreactive astrocytes treated with 3 days of control (B) or 10 mM NH_4 (C) conditions (scale bars, 20 microns). D) Average numbers of GFAP-immunoreactive astrocytes in sampled volumes showed no differences with ammonium exposure (n = 12; mean ± S.D.). E) Astrocytic volume, measured as the fraction of sampled volume positive for GFAP immunoreactivity, increased substantially with exposure to NH_4 1 – 10 mM, but not with exposure to 30 mM Na acetate (n = 12; mean ± S.D.; *$p<0.01$ compared to control conditions).

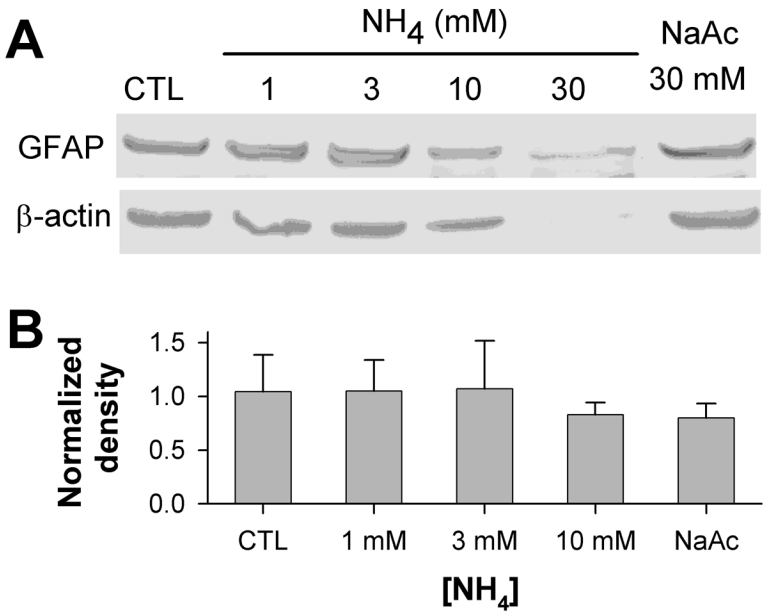

Figure 3. Immunoblotting for GFAP in ammonia-treated slices

A) Representative immunoblot of protein lysates from slices treated for 3 days in control conditions, with NH_4 acetate 1 – 30 mM, or with 30 mM Na acetate, probed for GFAP (upper panel) and re-probed for β-actin (lower panel). Immunoblotting detected single bands of ~ 50 kD for GFAP, and of ~ 42 kD for β-actin. B) Quantitation of GFAP band density, normalized to density of corresponding β-actin bands, detected no significant differences in GFAP content in samples from slices treated with 1–10 mM ammonia (n = 4; mean ± S.D.; p = 0.61). The 30 mM ammonia-treated samples, which showed large decreases in both GFAP and β-actin bands, were excluded from quantitation.

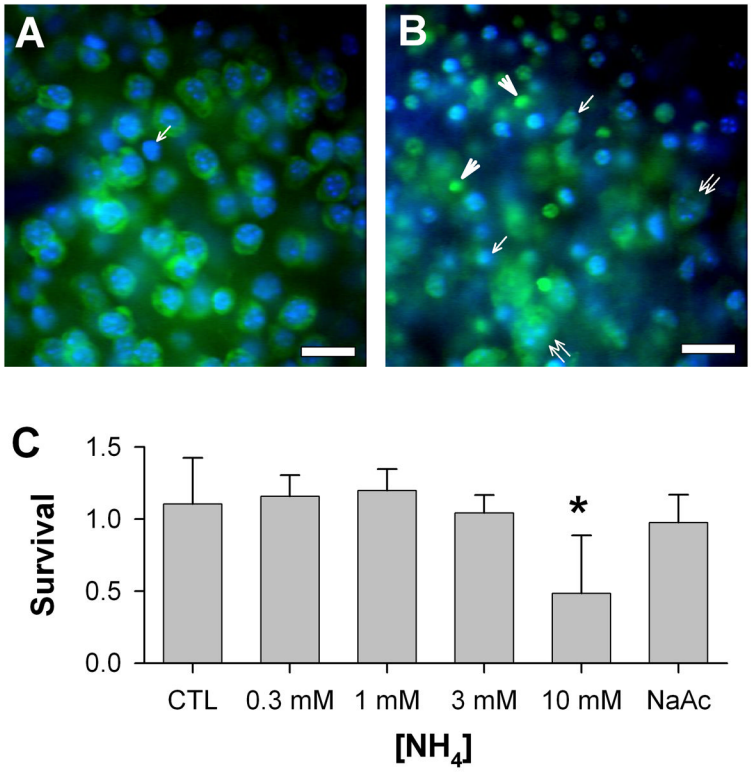

Figure 4. Neuronal changes in ammonia-treated cultured brain slices

Representative single confocal optical sections of Fluoro-Nissl staining of neurons in cultured slices (scale bars: 20 microns). A) Control slices showed plentiful neurons of regular size and morphology. Only rare nuclei lacked associated Fluoro-Nissl staining (arrow). B) After 10 mM ammonium acetate treatment, Fluoro-Nissl stained cells were irregular in size and shape, with both large, swollen cell somas containing swollen nuclei (double arrowheads) and shrunken, irregular cell profiles often with pyknotic nuclei (arrows). Other Nissl-stained objects lacked associated nuclei (arrowheads); these were not counted as surviving neurons. Pyknotic nuclei lacking surrounding Nissl-stained cytoplasm could also be seen. C) Blinded counting of surviving Nissl-positive neurons, showed a significant decrease in normalized neuronal survival in slices treated with 10 mM ammonia ($n = 6$; mean ± S.D.; $*p < 0.01$).